

Quantum Phase Transitions in Coupled Dimer Compounds

Om id Nohadani⁽¹⁾, Stefan Wessel⁽²⁾, and Stephan Haas⁽¹⁾

⁽¹⁾Department of Physics and Astronomy, University of Southern California, Los Angeles, CA 90089-0484 and

⁽²⁾Institut für Theoretische Physik III, Universität Stuttgart, 70550 Stuttgart, Germany

We study the critical properties in cubic systems of antiferromagnetically coupled spin dimers near magnetic-field induced quantum phase transitions. The quantum critical points in the zero-temperature phase diagrams are determined from quantum Monte Carlo simulations. Furthermore, scaling properties of the uniform magnetization and the staggered transverse magnetization across the quantum phase transition in magnetic fields are calculated. The critical exponents are derived from Ginzburg-Landau theory. We find excellent agreement between the quantum Monte Carlo simulations and the analytical results.

PACS numbers: 75.10.Jm, 73.43.Nq, 75.40.Cx

I. INTRODUCTION

Recent improvements in high magnetic field technology have made detailed investigations of quantum phenomena in strong magnetic fields possible. In particular, they allow for studies of quantum critical properties induced by high magnetic fields in weakly coupled spin dimer compounds, such as TiCuO_3 ^{1,2,3}, KCuO_3 ^{1,4}, $\text{BaCuSi}_2\text{O}_6$ ⁵, and $\text{Sr}_2\text{Cu}(\text{BO}_3)_2$ ⁶. The ground state of these materials consists of local spin singlets. If a magnetic field is applied that exceeds their singlet-triplet excitation gap, they undergo a transition into a magnetically ordered state. This quantum phase transition into a regime with transverse antiferromagnetic (AF) order can be described as a Bose-Einstein condensation (BEC) of triplet excitations, which behave as bosonic quasiparticles, called triplons. In the corresponding Bose-Hubbard model, this is analogous to the transition from the Mott-insulating phase to the superfluid condensate, where the magnetic field translates into the chemical potential. At very high magnetic fields, there is a saturation threshold, beyond which the spins fully align along the field direction, and the transverse antiferromagnetic order is destroyed. A schematic zero-temperature phase diagram is shown in Fig. 1. Because these compounds are three-dimensional, field-induced transverse antiferromagnetic order persists up to a finite transition temperature, $T_c(h)$, between the upper and lower critical field ($h_c < h < h_s$). Approaching the critical field from the partially polarized phase, $h \rightarrow h_c$, the critical temperature is expected to vanish as $T_c(h) \propto (h - h_c)^{1/3}$, with a universal power-law exponent that is predicted to be $\nu = 3/2$.^{7,8} While early experimental³ and numerical⁹ studies reported non-universal, i.e. coupling dependent, values of $\nu > 2$, it was recently shown in Ref. 10 that careful fitting of both experimental and numerical data indicates an effective exponent $\nu(h) > 3/2$, which approaches $3/2$ as $h \rightarrow h_c$. Motivated by this observation, Shindo and Tanaka¹¹ performed a fit of specific heat data in TiCuO_3 in the close vicinity of the lower critical field, yielding an exponent of $\nu = 1.67 \pm 0.07$. This value is closer to the universal value of $\nu = 3/2$ found in Ref. 10 than previous experimental

reports.

While numerical and experimental results on critical properties of the field-induced ordering transition agree well with analytical results at finite temperatures^{3,12}, there are no comparable scaling predictions for the zero-temperature quantum phase transitions. In this paper, we present a numerical analysis of critical properties in cubic systems of coupled dimers. In particular, zero-temperature scaling properties of the uniform and staggered magnetization in the partially polarized phase are studied, based on large-scale quantum Monte Carlo (QMC) simulations. These systems, upon increas-

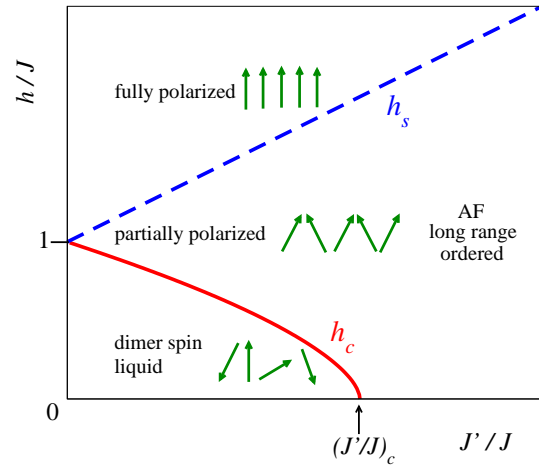


FIG. 1: Schematic zero-temperature phase diagram of a three-dimensional coupled dimer compound with intra-dimer couplings J and inter-dimer couplings J' . h denotes the strength of the external magnetic field.

ing the inter-dimer coupling, enter an antiferromagnetically ordered state at a quantum critical point ($J' = J$)_c.⁷ Magnetic exchange constants are known to depend sensitively on the distance between the magnetic sites. If their relative magnitudes are altered by the application of external pressure, such magnetic ordering transitions can be induced, as recently observed for TiCuO_3 .^{13,14} In this numerical study, the quantum critical point is determined for the structures shown in Fig. 2. Furthermore,

the quantum criticality induced by an applied magnetic field is studied. In particular, the scaling behavior of the uniform magnetization and the antiferromagnetic order parameter upon entering the partially polarized phase is determined. The associated critical exponents can be accessed experimentally and thus allow for a quantitative comparison.

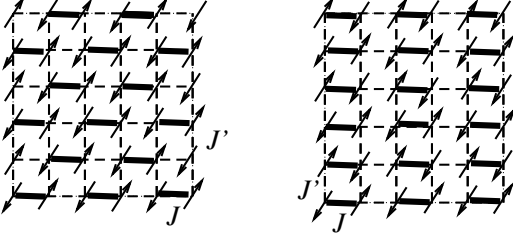


FIG. 2: Layers of coupled dimers, with staggered (left panel) and aligned (right panel) arrangements of dimers. The dimer bonds (J) are denoted by solid bars, whereas the inter-dimer bonds (J') are denoted by dashed lines. In the three-dimensional crystal, these layers are coupled by interlayer couplings of the same strength as J' . The arrangement of the dimers in neighboring layers is staggered (left panel), or aligned (right panel), respectively.

The paper is organized as follows: in the next section, the model used in the numerical simulations is defined and details about the quantum Monte Carlo method are presented. In Sec. III, the zero-temperature phase diagram of the system is discussed, and the quantum critical points at zero magnetic field are determined. A detailed scaling analysis of the magnetic properties at the quantum phase transitions in a magnetic field is presented in Sec. IV. Finally, conclusions are given in Sec. V. The Appendix contains a phenomenological derivation of the mean-field exponents, observed in Sec. IV, within Ginzburg-Landau theory.

II. MODEL AND METHOD

We consider the spin-1/2 Heisenberg antiferromagnet on the lattice structures shown in Fig. 2. The Hamiltonian is given by

$$H = \sum_{\langle ij \rangle} J_{ij} \mathbf{S}_i \cdot \mathbf{S}_j + h \sum_i S_i^z; \quad (1)$$

where the S_i denote localized spin-1/2 moments, and J_{ij} indicates the coupling constant between sites i and j , which takes values J for the dimer, and J' for the inter-dimer couplings. Furthermore, h denotes the applied magnetic field.

Since the lattice structures that are considered here, are bipartite (c.f. Fig. 2), antiferromagnetism in these systems is not frustrated, so that their properties can

be studied using large-scale QMC, without a sign-problem¹⁵. Here, we use the stochastic series expansion QMC method^{16,17} with directed loop updates^{18,19}. This update scheme results in higher sampling efficiency than other methods based on the conventional operator-loop update. Close to criticality, autocorrelation times are reduced by up to an order of magnitude. This allows detailed simulations of ground state properties on clusters with up to 10 000 sites, even in the presence of large magnetic fields. Furthermore, off-diagonal observables such as the transverse magnetic structure factor can be measured efficiently during the directed loop construction.^{19,20} Therefore, the order parameter in the partially polarized phase, i.e. the staggered transverse magnetization perpendicular to the magnetic field direction, can be calculated by using

$$m_s^? = \frac{r}{L^3} \frac{S_s^?}{L^3}; \quad (2)$$

Here, L denotes the linear system size and $S_s^?$ the transverse staggered structure factor,

$$S_s^? = \frac{1}{L^3} \sum_{\mathbf{h}; \mathbf{j}; \mathbf{i}} (1)^{i+j} \mathbf{h} S_i^x S_j^x; \quad (3)$$

These observables have been shown to saturate in QMC simulations at temperatures below $T = J^0/2L$, which is used throughout this study to ensure zero-temperature behavior.

III. ZERO-TEMPERATURE PHASE DIAGRAM

The zero-temperature phase diagram of coupled dimer systems in a magnetic field can be obtained using the bond-operator mean-field theory^{21,22}. A schematic phase diagram is shown in Fig. 1. It consists of three phases: (i) at low fields and small coupling ratios $J^0=J$, the system is in a magnetically disordered phase, i.e. a dimer spin liquid; (ii) at intermediate fields and/or sufficiently large values of $J^0=J$, the ground state is partially spin polarized and has an antiferromagnetic long-range order transverse to the magnetic field direction; and (iii) at large fields, $h > h_s = J + 5J^0$ all spins are fully polarized. These phase separations occur in both dimer arrangements, shown in Fig. 2.

While bond-operator theory provides a reliable description of the phase diagram¹⁰, a more precise estimate of the critical inter-dimer coupling strength, $(J^0=J)_c$, is required for the study of critical properties in finite magnetic fields, presented below. In order to determine this zero-field quantum critical point, we perform a finite-size scaling analysis of the staggered magnetization obtained from QMC simulations for various system sizes. Defining the dimensionless coupling ratio $g = J^0/J$, the relevant finite-size scaling is obtained as follows. The correlation length diverges near the quantum critical point g_c as

$\propto \sqrt{J - J_c}$. The correlation time τ_c during which fluctuations relax and decay (equilibration), is related to the correlation length $\xi_c \propto \sqrt{J - J_c}$, with the dynamical critical exponent z .²³ In the vicinity of the critical point and at zero-field, the staggered magnetization $m_s^2 = m_s$ for $g > g_c$ scales as

$$m_s \propto (g - g_c)^{\beta}; \quad (4)$$

defining an exponent β .²⁴ In general, this implies a finite-size scaling relation of the order parameter at the quantum critical point, $g = g_c$:

$$m_s / L^{\beta} = \text{const}. \quad (5)$$

Since these systems are explicitly dimerized, the Berry-phase contributions to the path-integral cancel.²⁵ Therefore, this QPT belongs to the universality class of the classical 3D Heisenberg model in 3+1 dimensions, with the dynamical critical exponent $z = 1$. Since the effective classical model is at the upper critical dimension ($d_c = 4$), the critical exponents β and ν take on mean-field values $\beta = 1/2$, $\nu = 0$, and the above scaling laws hold up to logarithmic corrections.⁷

A scaling plot of $m_s^2 L$ is shown in Fig. 3, using data from system sizes $L = 10$ to 20. On the scale of the main part of Fig. 3, a common intersection point of the finite-size data appears to exist. However, on a smaller scale, the insets of Fig. 3 exhibit the logarithmic corrections to Eq. (5). With increasing system size, we observe that the intersections for neighboring system sizes move towards increasing values of $(J^0 = J)_c$. As seen in inset (b) of Fig. 3, the systematic increase of the crossing points scales well as a function of $1/L^2$, which allows us to extrapolate the thermodynamic limit value of $(J^0 = J)_c = 0.2492 \pm 0.0002$ for the quantum critical point. These logarithmic corrections are best accessible when system sizes of different orders of magnitude are compared. However, because of computational restrictions, we follow the approach described above.

Performing a similar analysis for the staggered configuration of dimers in Fig. 2(a), we find the quantum critical point at $(J^0 = J)_c = 0.2170 \pm 0.0002$. This lower critical inter-dimer coupling for the staggered configuration indicates a reduced tendency towards the formation of dimer singlets for this arrangement of dimers, as compared to the aligned dimer configuration.

Beyond the critical inter-dimer coupling, the staggered magnetization increases with a mean-field exponent $\beta = 1/2$, as in Eq. (4). The QMC data of m_s , shown in Fig. 4, are consistent with this scaling behavior. However, due to restricted system sizes, we are not able to extract the logarithmic corrections to the scaling law.

IV. FIELD-INDUCED QUANTUM PHASE TRANSITION

Having determined the quantum critical points of coupled-dimer arrays, we proceed to study the effects of a

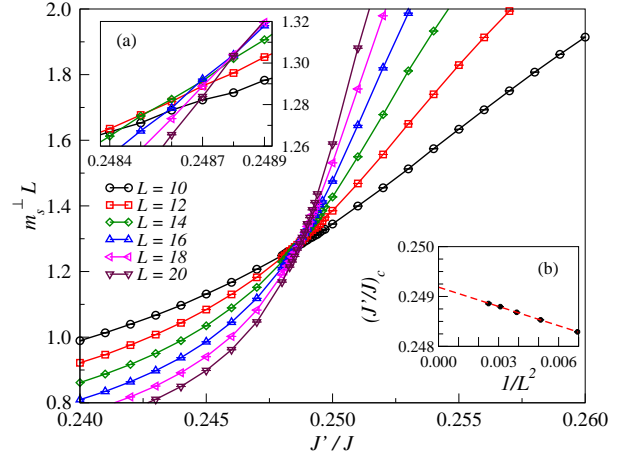


FIG. 3: Scaling plot of the zero-temperature staggered magnetization in the aligned arrangement of Fig. 2 (b) obtained from quantum Monte Carlo simulations using systems of linear sizes $L = 10$ to 20. J denotes the intra-dimer coupling. At the critical inter-dimer coupling $(J^0 = J)_c$, the different curves intersect each other (main panel). Inset (a) shows a magnification of the intersection region. Inset (b) exhibits the corrections to the mean-field scaling behavior, arising from logarithmic corrections in the upper critical dimension. The statistical error bars fall within the symbol size.

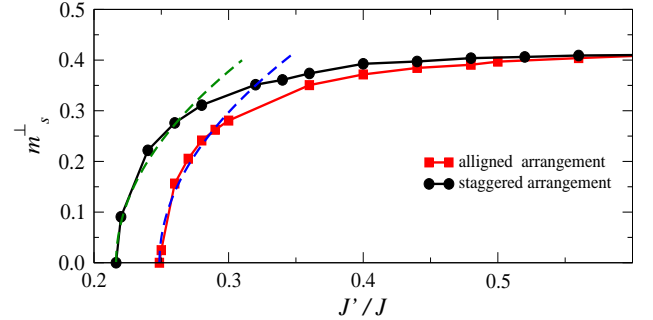


FIG. 4: Staggered magnetization m_s of coupled dimer arrays as a function of the inter-dimer coupling strength J^0 , for the two different dimer arrangements of Fig. 2. Dashed lines show the mean-field scaling behavior with exponent $\beta = 1/2$ close to the quantum critical point.

magnetic field in the different regimes. In particular, we determine the scaling behavior of the uniform magnetization and the order parameter upon entering the partially polarized region. The corresponding scaling exponents are accessible experimentally by direct measurement of the magnetization, and by neutron scattering. Thus, the numerical results can be compared with analytical predictions and with measurements on the materials mentioned above. Here, simulations for the aligned configuration of dimers, shown in Fig. 2(b), are presented. For the staggered configuration of dimers, the same scaling exponents are obtained. This is due to the underlying universality.

A . Scaling of the Uniform Magnetization

First, we discuss the behavior of the uniform magnetization $m_u(h)$ as a function of the applied magnetic field. In the dimer spin liquid phase, i.e. for coupling ratios smaller than $(J^0=J)_c$, a finite magnetic excitation gap separates the ground state singlet and the lowest triplet state. Thus, a finite magnetic field $h_c =$ is required to close this gap, and to induce a finite uniform magnetization. The Ginzburg-Landau approach presented in Appendix A predicts m_u to increase linearly, $m_u / (h - h_c)$ for $h > h_c =$ and for $J^0 < J_c^0$. When the inter-dimer coupling is increased, the gap becomes smaller, until it vanishes at the critical inter-dimer coupling J_c^0 . At the quantum critical point, $J^0 = J_c^0$, the Ginzburg-Landau approach predicts the uniform magnetization to scale as m_u / h^3 : For larger values of $J^0 > J_c^0$, the excitation gap remains zero, and the finite uniform susceptibility χ_u results in a linear response $m_u = \chi_u h$ of the uniform magnetization in the Neel-ordered regime beyond J_c^0 .

Let us now compare these predictions with the QMC results obtained from simulations of systems with linear sizes up to $L = 30$. For such large system sizes, we did not detect finite-size effects in the uniform magnetization. In Fig. 5, results for various values of the inter-dimer coupling strength are presented. The main part of Fig. 5 shows the uniform magnetization over the full range of magnetic field strengths, up to the saturation field $h_s = J + 5J^0$. Inset (a) of Fig. 5 focuses on the region close to the critical field h_c for various inter-dimer couplings J^0 . The linear scaling in h , which is predicted on both sides of the quantum critical point, is clearly observed in this small m_u region. In contrast, at the quantum critical point, $J^0 = J_c^0$, the uniform magnetization increases non-linearly with h , as shown in Fig. 5 (a). Indeed, we observe a scaling m_u / h^3 , presented in Fig. 5 (b). This is expected from the Ginzburg-Landau theory (c.f. Appendix A) and the bond-operator mean-field theory²². Using QMC, these scaling exponents of the uniform magnetization are verified.

Finally, we note that the field dependence of m_u for the entire region between h_c and h_s is linear for weakly coupled dimers (see e.g. Fig. 5 for $J^0 = 0.07J$), consistent with bond-operator mean-field theory²². For larger values of J^0 , m_u shows deviations from this linear behavior in high magnetic fields. This non-linear behavior can be accounted for within bond-operator theory by including the contributions of higher-energy triplet modes to the ground state²².

B . Scaling of the Order Parameter

Next, we discuss the scaling properties of the order parameter in the partially polarized phase, i.e. the staggered transverse magnetization perpendicular to the magnetic field direction, $m_s^z(h)$, as a function of the applied magnetic field h . Before presenting numerical data,

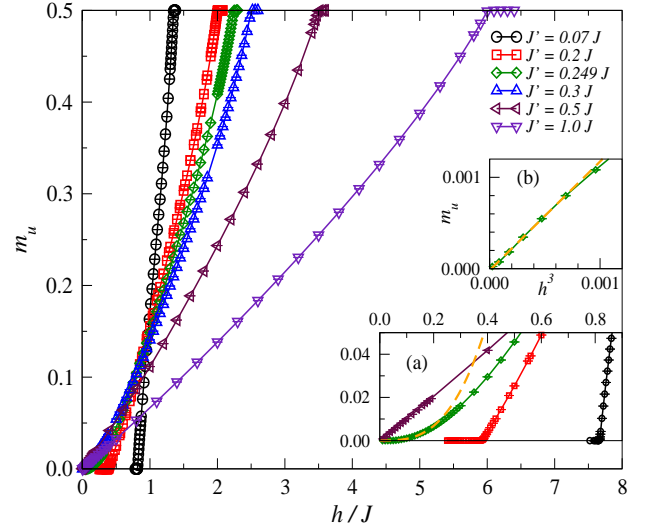


FIG. 5: Zero-temperature uniform magnetization of aligned dimer arrays for different inter-dimer couplings as a function of the magnetic field h . Inset (a) focuses on the low-field region, $h=J < 1$. The scaling m_u / h^3 at $J^0 = J_c^0$ is demonstrated in inset (b).

the expectations from the Ginzburg-Landau theory from Appendix A can be summarized as following. For $J^0 < J_c^0$ and magnetic fields $h > h_c =$, $m_s^z / (h - h_c)$ is expected, consistent with bond-operator mean-field theory²². At the critical inter-dimer coupling, $J^0 = J_c^0$, a linear relation m_s^z / h is expected. Within the antiferromagnetically ordered regime, $J^0 > J_c^0$, a finite staggered magnetization $m_s^z = m_s$ exists. For small fields, the order parameter scales with $m_s^z = m_s / h^2$, as presented in Ref. 22.

QMC calculations of m_s^z for different values of $J^0=J$ in a system with $L = 16$ are shown in Fig. 6. This Figure demonstrates that for $J^0 < J_c^0$, the staggered magnetization is largest for $h = (h_c + h_s)/2$ and decreases upon approaching h_c and h_s . In the thermodynamic limit, m_s^z vanishes in the fully polarized regime, $h > h_s$ and below h_c for weakly coupled dimers. In contrast to the uniform magnetization, the field dependence of m_s^z shows a strong finite-size dependence. Finite-size effects are most pronounced for magnetic field regimes outside the partially polarized phase, i.e. for $h < h_c$ and $h > h_s$, where $m_s^z = 0$ in the thermodynamic limit. On the finite systems accessible to QMC, the values of m_s^z , defined in Eq. (2) do not vanish. However, they scale to zero upon increasing the system size. In order to extract the scaling behavior of m_s^z , we thus need to perform a careful finite-size scaling analysis of the numerical data.

Such an analysis can be directly applied in the weak coupling regime, for $J^0 < J_c^0$. Here, the field-induced ordering transition is known to constitute a Bose-Einstein condensation of triplons,⁷ with a dynamical critical exponent $z = 2$, reflecting the quadratic dispersion relation of these bosonic excitations. Therefore, the quantum phase transition at the critical field h_c is in the universality

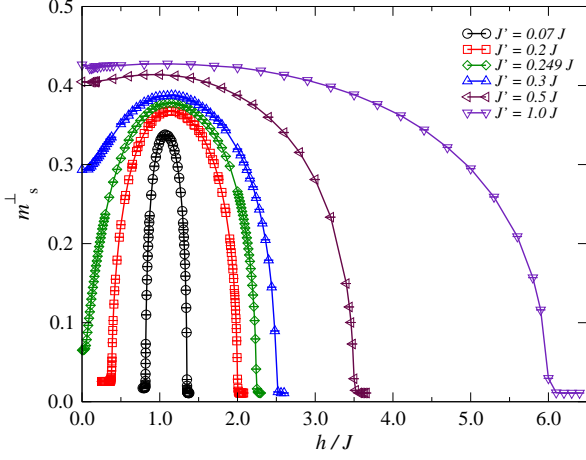


FIG. 6: Zero-temperature staggered transverse magnetization m_s^z in coupled aligned dimer arrays as a function of an applied magnetic field h . Quantum Monte Carlo data of a $16 \times 16 \times 16$ system are shown for different values of the inter-dimer coupling J^0 . The intra-dimer coupling is denoted by J . The \circ -sets of m_s^z outside the range $h_c < h < h_s$ are due to finite-size effects.

class of the classical 5-dimensional $O(2)$ model, and a finite-size scaling analysis similar to the one performed for the zero-field quantum critical point in Sec. IV A can be applied. Since the classical theory is now above $d_c = 4$, mean-field scaling without logarithmic corrections applies. In particular, at the critical field h_c , one finds

$$m_s^z L / F(L^{-1/2}) ; \quad (6)$$

where F is a scaling function that depends on the ratio of the correlation length and the system size L . In order to determine h_c for a given value of $J^0 < J_c$, we can thus construct a scaling plot of $m_s^z L$ as a function of h/J . Fig. 7 illustrates an example of such a plot for an inter-dimer coupling $J^0 = 0.2J$. In Fig. 7(a), data for $m_s^z L$ are shown for system sizes $L = 10, 14, 18$, and 20 . The intersection point of the different finite-size data allows the extraction of the critical field $h_c = 0.383 \pm 0.001$ for this value of $J^0 = 0.2J$.

Once the critical field h_c is determined, data collapse of the finite-size data is verified in the vicinity of h_c . Namely, from the scaling of the correlation length close to the critical field, $\xi \sim |h - h_c|^{-\nu}$, one obtains

$$m_s^z L / \tilde{F}(L^{1-\nu} |h - h_c|) ; \quad (7)$$

with a new scaling function \tilde{F} and $\nu = 1/2$. An example of the data collapse for $J^0 = 0.2J$ is shown in Fig. 7(b).

In order to extract the behavior of $m_s^z(h)$ for $h > h_c$ in the thermodynamic limit, we perform an extrapolation of the finite-size data $m_s^z(L)$ as a function of $1/L$. An example of such an extrapolation, again for $J^0 = J = 0.2$ is shown in Fig. 8 for various values of h . While for h close to h_c , a linear scaling in $1/L$ is obtained, extrapolation away from h_c requires the use of higher order

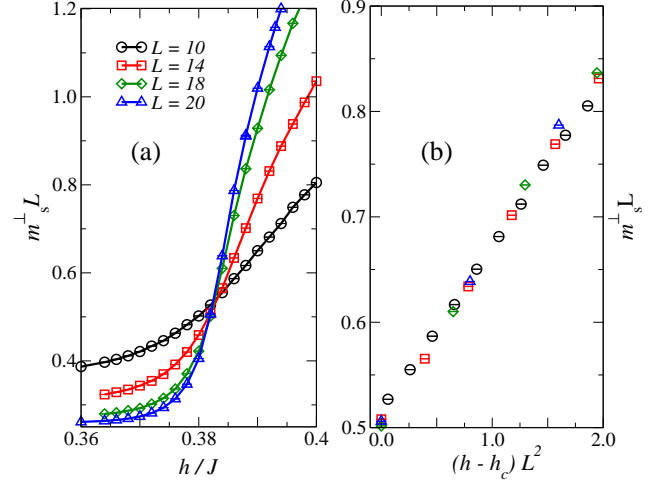


FIG. 7: Scaling plot (a) and data collapse (b) for the zero-temperature staggered transverse magnetization m_s^z of weakly coupled aligned dimers as a function of the applied magnetic field h for a coupling-ratio of $J^0 = J = 0.2$. Results from quantum Monte Carlo simulations are shown for system sizes of $L = 10$ to 20 .

polynomials. Using these extrapolated values of $m_s^z(h)$, representing the thermodynamic limit, we then obtained the scaling behavior of $m_s^z(h)$ shown for different values of $J^0 = J$ in Fig. 9.

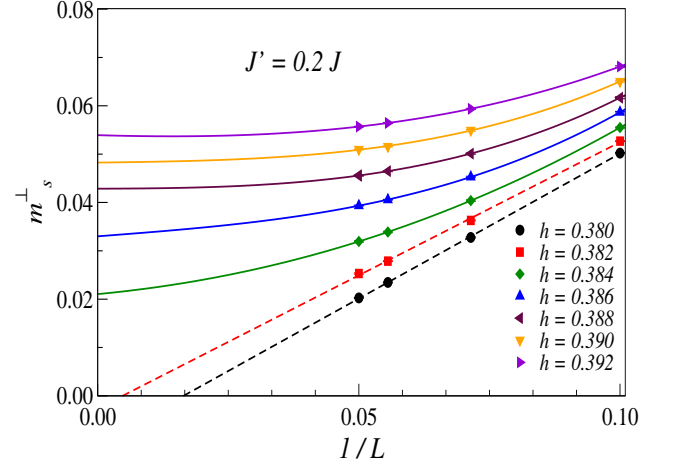


FIG. 8: Extrapolation of finite-size data of staggered magnetization for different magnetic fields close to the transition. At h_c , thermodynamic limit is obtained from a $1/L$ -extrapolation. Higher order polynomials are required away from criticality. For all data presented here, up to the third order is used. Dashed lines are for $h < h_c$.

For weakly coupled dimers with $J^0 = 0.07J$ Fig. 9(a) exhibits a scaling of $m_s^z \sim |h - h_c|^{-1/2}$. The scaling exponent $1/2$ is also found for stronger inter-dimer couplings, as shown in Fig. 9(b) for $J^0 = 0.2J$. This square root dependence $m_s^z \sim |h - h_c|^{-1/2}$ is consistent with the analytical results and expected from the mean-field value $\nu = 1/2$.

Next, let us consider the scaling of $m_s^z(h)$ for a criti-

cal inter-dimer coupling $J^0 = J_c^0$. In Fig. 9(c), we show results from simulations at the critical point $J^0 = 0.249$. Here, a linear scaling m_s^2 / h is observed, consistent with the Ginzburg-Landau calculations from Appendix A. Finally, we consider the Neel-ordered phase ($J^0 > J_c^0$). The results from the extrapolated QMC data is shown for $J^0 = 0.3J$ in Fig. 9(d). Increasing the magnetic field, a non-linear increase of $m_s^2(h)$ from its zero-field value m_s is found, which can be fitted well to the analytical prediction, $m_s^2(h) = m_s^2 + m_s^2 h^2$. We thus obtain agreement of the QMC data with the analytical results based on Ginzburg-Landau and bond-operator mean-field theory also for the scaling of the order parameter.

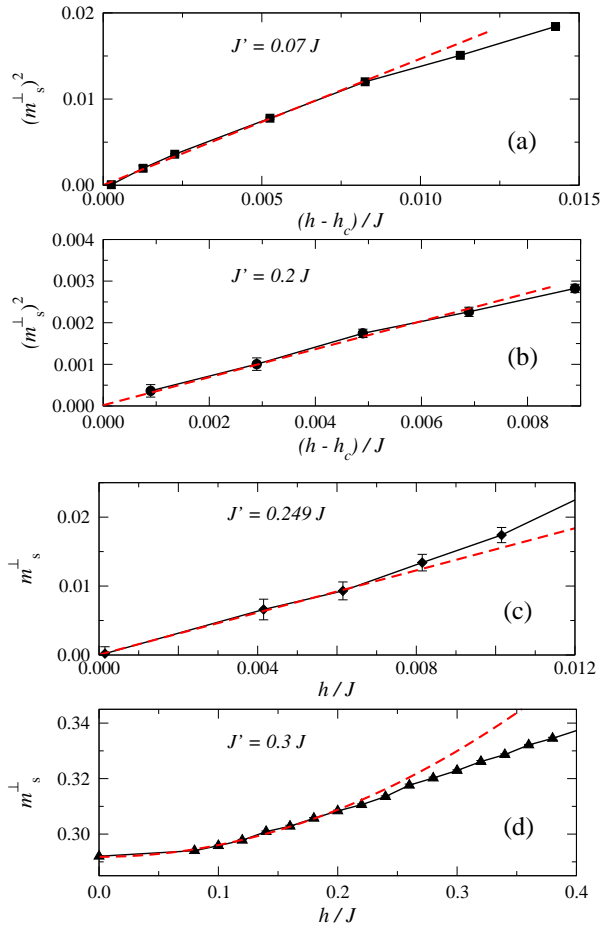


FIG. 9: Scaling behavior of the zero-temperature staggered transverse magnetization as a function of the applied magnetic field h . Quantum Monte Carlo data are shown after extrapolation of finite-size data ($L = 10 - 20$) to the thermodynamic limit. (a) (b) in the dimer spin liquid phase ($J^0 < J_c^0$), $(m_s^2)^2$ scales linear with $h - h_c$. (c) near the critical coupling (J_c^0), m_s^2 scales linear with $h - h_c$. (d) for $J^0 > J_c^0$, m_s^2 increases quadratically with h .

V. SUMMARY

We examined quantum phase transitions in three-dimensional coupled dimer arrays. The zero-temperature phase diagrams of these systems feature a low-field dimer spin liquid phase at weak inter-dimer couplings, a partially polarized regime with long-range transverse magnetic order for intermediate magnetic fields $h_c < h < h_s$, and a fully polarized phase at high magnetic fields.

The critical exponents associated with quantum phase transitions between these regimes were extracted using finite-size scaling analysis of quantum Monte Carlo data. The numerical values of these exponents compare well with Ginzburg-Landau calculations and bond-operator mean-field theory. In particular, for small inter-dimer coupling, the order parameter is found to scale as $(h - h_c)^{1/2}$, whereas the uniform magnetization scales linear in $h - h_c$. Moreover, at the quantum critical point ($J^0 = J_c^0$), we demonstrated linear scaling for m_s^2 / h . In a recent magnetization study on the TiCuCl_3 system under hydrostatic pressure¹⁴, a cubic scaling of the uniform magnetization m_u / h^3 at the critical value of the applied pressure was observed. This is in perfect agreement with numerical results and analytical predictions based on Ginzburg-Landau calculations and bond-operator theory.

We found that corrections to mean-field scaling emerge at the zero-field pressure-induced quantum phase transition, such as those in Ref. 13,14. For example, in Ref. 14, the pressure-dependence of the gap was fitted to a power law with an exponent 0.445, while the mean-field theory predicts an exponent 0.5, without taking logarithmic corrections into account.²² Assuming a linear scaling of the pressure P with the inter-dimer interactions,¹⁴ close to the critical point P_c , we find the scaling of the gap to be

$$\Delta / \Delta_c = \Delta_c / (P - P_c)^{1/2} \quad \ln \frac{P - P_c}{P_c} \approx 1/6 \quad (8)$$

from a renormalization group analysis of the classical $d = 4$ -theory at $d_c = 4$ ²⁶. Therefore, careful fitting of experimental data can exhibit the logarithmic corrections near quantum critical points in three-dimensional compounds.

Acknowledgment

We thank Andreas Honecker, Bruce Normand, Tomaso Roscilde, Subir Sachdev, Manfred Sigrist, Hidekazu Tanaka, Matthias Troyer, and Matthias Vojta for useful discussions. Furthermore, we acknowledge financial support from NSF Grant No. DMR-0089882. Computational support was provided by the USC Center for High Performance Computing and Communications. Parts of the numerical simulations were performed using the ALPS project library.²⁷

APPENDIX A: GINZBURG-LANDAU THEORY

In this Appendix, we present a phenomenological Ginzburg-Landau description of weakly coupled dimers in a magnetic field²⁸, and derive the scaling exponents of the uniform magnetization m_u and the order parameter m_s in the partially polarized phase.

Due to rotational symmetry within the plane perpendicular to the external field, the free energy of the system can be expanded as

$$F = a(h; J^0) (m_s^?)^2 + b (m_s^?)^4; \quad (A1)$$

neglecting higher orders of $m_s^?$ in the vicinity of the critical field.²⁹ Here, $a(h; J^0)$ vanishes for h equal to the critical magnetic field $h = h_c(J^0)$. Taking into account time reversal symmetry, a can be expressed as $a = \bar{a} (h - h_c^2(J^0))$. The staggered magnetization $m_s^?$ and the uniform magnetization m_u is obtained from Eq. A1 as

$$\frac{\partial F}{\partial m_s^?} = 0 \text{ and } m_u = \frac{\partial F}{\partial h} : \quad (A2)$$

From this, one finds

$$m_s^? = \frac{\bar{a} (h^2 - h_c^2)}{2b} \quad (A3)$$

$$m_u = 2\bar{a}h (m_s^?)^2 : \quad (A4)$$

To proceed further, we distinguish two regions, namely weak inter-dimer couplings ($J^0 < J_c^0$) and the quantum critical point ($J^0 = J_c^0$). For the first region, (A3) can be expanded in terms of the distance to the lower critical field, i.e. $h - h_c$. One obtains

$$\text{for } J^0 < J_c^0 : \quad m_s^? = \frac{\bar{a} (h + h_c) (h - h_c)}{2b}; \quad (A5)$$

$$) \quad m_s^? \propto (h - h_c)^{1/2}; \quad (A5)$$

$$) \quad m_u \propto 2\bar{a}h (h - h_c)^{1/2} : \quad (A6)$$

At the critical inter-dimer coupling the critical field is zero. Therefore,

$$\text{for } J^0 = J_c^0 : \quad m_s^? = \frac{\bar{a}}{2b} h; \quad (A7)$$

$$) \quad m_u \propto 2\bar{a}h^3 : \quad (A8)$$

These exponents agree with the numerical data presented in the preceding sections, as well as previous bond-operator mean-field theory results²².

- ¹ W. Shiramura, K. Takatsu, H. Tanaka, K. Kamishima, M. Takahashi, H. M. Iitama, and T. Goto, J. Phys. Soc. Jpn. 66, 1900 (1997).
- ² A. Osawa, M. Ishii, and H. Tanaka, J. Phys. Condens. Matter 11, 265 (1999); N. Cavadini, G. Heigold, W. Henggeler, A. Furrer, H.-U. Gudel, K. Kramer, and H. Mütka, Phys. Rev. B 63, 172414 (2001); Ch. Ruegg, N. Cavadini, A. Furrer, H.-U. Gudel, K. Kramer, H. Mütka, A. Wildes, K. Habicht, and P. Vorderwisch, Nature (London) 423, 62 (2003).
- ³ H. Tanaka, A. Osawa, T. Kato, H. Uekusa, Y. Ohashi, K. Kakurai, and A. Hoser, J. Phys. Soc. Jpn. 70, 939 (2001).
- ⁴ T. Kato, K. Takatsu, H. Tanaka, W. Shiramura, M. Mori, K. Nakajima, and K. Kakurai, J. Phys. Soc. Jpn. 67, 752 (1998); A. Osawa, T. Takamasu, K. Tatani, H. Abe, N. Tsujii, O. Suzuki, H. Tanaka, G. Kido, and K. Kido, Phys. Rev. B 66, 104405 (2002).
- ⁵ M. Jaime, V. F. Correa, N. Harrison, C. D. Batista, N. Kawashima, Y. Kazuma, G. A. Jorge, R. Stem, I. Heinmaa, S. A. Zvyagin, Y. Sasago, and K. Uchinokura, Phys. Rev. Lett. 93, 087203 (2004).
- ⁶ S. Sebastian, D. Yin, P. Tanedo, G. A. Jorge, N. Harrison, M. Jaime, Y. Mozharivskyj, G. Miller, J. Krzystek, S. A. Zvyagin, and I. R. Fisher, Report cond-mat/0403334.
- ⁷ S. Sachdev, Quantum Phase Transitions, (Cambridge University Press, 1999).
- ⁸ N. Kawashima, Report cond-mat/0408649.

- ⁹ S. Wessel, M. Oshani, and S. Haas, Phys. Rev. Lett. 87, 206407 (2001).
- ¹⁰ O. Nohadani, S. Wessel, B. Normand, and S. Haas, Phys. Rev. B 69, 220402 (2004).
- ¹¹ Y. Shindo and H. Tanaka, J. Phys. Soc. Jpn. Vol.73 No.10 (2004).
- ¹² T. Giamarchi and A. M. Tsvelik, Phys. Rev. B 59, 11398 (1999); T. Nikuni, M. Oshikawa, A. Osawa, and H. Tanaka, Phys. Rev. Lett. 84, 5868 (2000).
- ¹³ A. Osawa, M. Fujisawa, T. Osakabe, K. Kakurai, and H. Tanaka, J. Phys. Soc. Jpn. Vol.72 No.5 (2003).
- ¹⁴ K. Goto, M. Fujisawa, T. Ono, H. Tanaka, and Y. Uwatoko, J. Phys. Soc. Jpn. Vol.73 No.12 (2004).
- ¹⁵ M. Troyer and U.-I. Wiesse, Report cond-mat/0408370.
- ¹⁶ A. W. Sandvik, Phys. Rev. B 59, R14157 (1999).
- ¹⁷ A. W. Sandvik, Phys. Rev. B 56, 11678 (1997); A. W. Sandvik, Phys. Rev. Lett. 80, 5196 (1998).
- ¹⁸ O. F. Syljåsen and A. W. Sandvik, Phys. Rev. E 66, 046701 (2002).
- ¹⁹ F. Alet, S. Wessel, and M. Troyer, Report cond-mat/0308495.
- ²⁰ A. Dornreich and M. Troyer, Phys. Rev. E 64, 066701 (2001).
- ²¹ M. Matsumoto, B. Normand, T. M. Rice, and M. Sigrist, Phys. Rev. Lett. 89, 077203 (2002).
- ²² M. Matsumoto, B. Normand, T. M. Rice, and M. Sigrist, Phys. Rev. B 69, 054423 (2004); B. Normand, M. Mat-

- sumoto, O. Nohadani, S. Wessel, S. Haas, T. M. Rice, and M. Sigrist, *J. Phys.: Condens. Matter* **16**, No 11, S867–S873 (2004).
- ²³ M. Vojta, *Rep. Prog. Phys.* **66**, 2069 (2003). A. V. Chubukov, S. Sachdev, and J. Ye, *Phys. Rev. B* **49**, 11919 (1994). S. Chakravarty, B. I. Halperin, and D. R. Nelson, *Phys. Rev. Lett.* **60**, 1057 (1988); *Phys. Rev. B* **39**, 2344 (1989). Troyer and M. Imada, *Computer Simulations in Condensed Matter Physics X*, eds. D. P. Landau et al., (Springer Verlag, Heidelberg, 1997).
- ²⁴ M. Troyer, M. Imada and K. Ueda, *J. Phys. Soc. Jpn.* **66**, 2957 (1997). M. Troyer and M. Imada, *Computer Simulations in Condensed Matter Physics X*, eds. D. P. Landau et al., (Springer Verlag, Heidelberg, 1997).
- ²⁵ T. Senthil, et al. *Science* **303**, 1490 (2004); and references therein.
- ²⁶ J. Zinn-Justin, *Quantum Field Theory and Critical Phenomena*, Oxford University Press, 2002.
- ²⁷ M. Troyer et al.: *Lecture Notes in Computer Science* **1505** (1998) 191; F. Alet et al., *Report cond-mat/0410407*. Sources of this library are available at <http://alps.comp-phys.org/>.
- ²⁸ M. Matsumoto and M. Sigrist, *Report cond-mat/0401411*.
- ²⁹ I. S. Aranson and L. Kramer, *Rev. of Mod. Phys.* **74**, 99–143 (2002).